An NMR Crystallographic Investigation of the Relationships between the Crystal Structure and 29Si Isotropic Chemical Shift in Silica Zeolites

Daniel M. Dawson,* Robert F. Moran and Sharon E. Ashbrook*

School of Chemistry, EaStCHEM and Centre for Magnetic Resonance, University of St Andrews, North Haugh, St Andrews KY16 9ST, UK

*Author to whom correspondence should be addressed.

Electronic mail: *dmd7@st-andrews.ac.uk, sema@st-andrews.ac.uk*

Abstract

NMR crystallography has recently been applied to great effect for silica zeolites. Here we investigate whether it is possible to extend the structural information available from routine NMR spectra *via* a simple structure-spectrum relationship. Unlike previous empirically-derived relationships that have compared experimental crystal structures for (often disordered) silicates with experimental NMR spectra, where the structure may not be an accurate representation of the material studied experimentally, we use NMR parameters calculated by density functional theory (DFT) for both model $Si(OSi(OH)_3)_4$ clusters and also extended zeolitic SiO_2 frameworks, for which the input structure corresponding to the NMR parameters is known exactly. We arrive at a structure-spectrum relationship dependent on the mean Si–O bond length, mean Si–O–Si bond angle, and the standard deviations of both parameters, which can predict to within 1.3 ppm the ^{29}Si isotropic magnetic shielding that should be obtained from a DFT calculation. While this semi-empirical relationship will never supersede DFT where this is possible, it does open up the possibility of a rapid estimation of the outcome of a DFT calculation where the actual calculation would be prohibitively costly or otherwise challenging. We also investigate the structural optimisation of SiO_2 zeolites using DFT, demonstrating that the mean Si–O bond lengths all tend to 1.62 Å and the distortion index tends to <2.0°, suggesting that these metrics may be suitable for rapid validation of whether a given crystal structure represents a realistic local geometry around Si, or merely a bulk average with contributions from several different local geometries.

Introduction

^{29}Si NMR spectroscopy has long been a key tool in the structural characterisation of silicate-based zeolites, owing to its moderate natural abundance and receptivity, spin quantum number I = 1/2 and, most importantly, its sensitivity to small changes in the local structure.[1-3] It is, for example, well known that the ranges of chemical shifts observed for $Si(OH)_{4-n}(OT)_n$ (*i.e.*, Q^n silicate species, where T = Si) are distinct for different values of n and, in aluminosilicate zeolites, the chemical shift for a given Q^n Si species differs by ~7 ppm per next-nearest neighbour Al atom substituted on the T site.[3,4] In one of the most important recent examples of the power of solid-state NMR spectroscopy to provide structural information on silicate zeolites, Brouwer *et al*. demonstrated that it is possible to solve such structures using only a unit cell determined from crystallographic measurements and the build-up curves from ^{29}Si double-quantum NMR experiments to provide distance restraints.[5] However, this sort of approach is extremely time consuming, owing to the requirement to record a series of experiments where [29]Si double-quantum coherences must be excited between spin pairs at natural abundance (*i.e.*, only 0.22% of all Si pairs). It would, therefore, be desirable to have some means of extracting information from the simple one-dimensional ^{29}Si MAS NMR spectra of zeolites and relating this in some way to their structure.

In the past, this goal has led to many proposed links between the [29]Si isotropic chemical shift, δ_{iso}, and a variety of structural parameters including the mean Si-O-Si bond angle ($\langle\theta_{SiOSi}\rangle$, in °) and the mean Si–O bond length ($\langle r_{SiO}\rangle$ in Å) in a range of silicate minerals, zeolites and glasses.[3] Examples include the relationship based on a set of 20 silicates with δ_{iso} = 875 $\langle r_{SiO}\rangle$ – 1509, albeit with substantial scatter[6] and a set of four silica polymorphs and a silicalite precursor that exhibit a very different relationship of δ_{iso} = 325.8 $\langle r_{SiO}\rangle$ – 633.[7] Other relationships proposed between [29]Si δ_{iso} and $\langle r_{SiO}\rangle$ are typically closer to the former than the latter, with δ_{iso} = 1447 $\langle r_{SiO}\rangle$ – 2432 for sodium and potassium feldspars,[8] δ_{iso} = 1218 $\langle r_{SiO}\rangle$ – 2058 for several silicates and quartz,[9] δ_{iso} = 1372$\langle r_{SiO}\rangle$ – 2312 for albite, natrolite and two silica polymorphs,[10] δ_{iso} = 1187 $\langle r_{SiO}\rangle$ – 2014 for a selection of

silicates[11] and δ_{iso} = 1126 $\langle r_{SiO} \rangle$ – 1909 for Mg_2SiO_4,[12] leading to a range of descriptions that follow the same general trend, *i.e.*, δ_{iso} moves downfield as $\langle r_{SiO} \rangle$ increases. Hochgräfe *et al.* used this trend to great effect in the assignment of [29]Si resonances in a three siliceous zeolites.[13] However, these relationships typically exhibit significant scatter, as shown in Figure 1a, which suggests that the dependence on a single parameter may be an oversimplification. This is not surprising, given the range of materials from which data points have been taken, the uncertainty associated with the structural parameters and the fact that these relationships aim to describe the magnetic shielding interaction by a single structural parameter.

Similarly, given it is known that the electronegativity of the Si–O bond relates to the Si–O–Si bond angle,[3] many relationships (as shown in Figure 1b) have been reported between [29]Si δ_{iso} and the mean Si-O-Si bond angle, $\langle \theta_{SiOSi} \rangle$. These relationships include δ_{iso} = –0.603 $\langle \theta_{SiOSi} \rangle$ – 20.8 for four silica polymorphs and a silicalite precursor,[7] δ_{iso} = –1.17 $\langle \theta_{SiOSi} \rangle$ + 68.6 for sodium and potassium feldspars,[8] δ_{iso} = –0.619 $\langle \theta_{SiOSi} \rangle$ – 18.7 for 13 silica polymorphs and zeolites,[14] δ_{iso} = –0.533 $\langle \theta_{SiOSi} \rangle$ – 10.7 for $Si(OAl)_4$ in nine zeolites,[15] δ_{iso} = –0.579$\langle \theta_{SiOSi} \rangle$ – 25.3 for six zeolites,[16] δ_{iso} = –0.563 $\langle \theta_{SiOSi} \rangle$ – 9.62 for three sodium disilicate polymorphs,[17] δ_{iso} = –0.686 $\langle \theta_{SiOSi} \rangle$ – 8.29 for $Si(OSi)_4$ in three zeolites,[18] δ_{iso} = –0.609 $\langle \theta_{SiOSi} \rangle$ – 20.6 for silicalite-1,[19] δ_{iso} = –0.79 $\langle \theta_{SiOSi} \rangle$ + 18.18 for 13 leucites and related compounds,[20] and δ_{iso} = –0.62 $\langle \theta_{SiOSi} \rangle$ – 1.09 for 33 sodalites with different cage contents.[21] Müller *et al.* reported a gradient of –0.57 ppm per degree for three dense phases of SiO_2 when combined with data for the isostructural $AlPO_4$ phases,[22] although for just the SiO_2 phases (using numerical data from Smith and Blackwell[7]), the relationship is δ_{iso} = –0.622 $\langle \theta_{SiOSi} \rangle$ – 17.8. As in the case of the relationship between [29]Si δ_{iso} and $\langle r_{SiO} \rangle$, although there is a general trend for a decrease in δ_{iso} with increasing $\langle \theta_{SiOSi} \rangle$, there is a large variation in the gradients and y-intercepts for the assumed linear correlations. It is clear from Figure 1b that the data discussed above generally fall into several sets of near-parallel lines, but with significant scatter for each grouping.

Relationships between [29]Si δ_{iso} and several other geometric and geometric-electronic

parameters have also been investigated, including the mean Si-T distance (T = Si, Al, Ge, *etc.*),[7,20] the mean O–Si–O angle, $\langle \theta_{OSiO} \rangle$,[7-9] $\sec(\langle \theta_{SiOSi} \rangle)$ and $\cos(\langle \theta_{SiOSi} \rangle)/[1-\cos(\langle \theta_{SiOSi} \rangle)]$,[7,14,15,17,23] and the bond strengths or electronegativities of the adjacent T cations (later modified to account for variation in the Si–O–X angles).[6,8,11,12,14,19,24,25] Sherriff *et al.* proposed a more complicated but, in principle, universally applicable relationship, where the major contribution to the ^{29}Si shielding was assumed to be from the magnetic susceptibility of the bond between O and the next-nearest neighbour T atom.[26] Their relationship

$$\delta_{iso} = 701.6\,\Omega' - 45.7\,, \tag{1}$$

where,

$$\Omega' = \sum_{i=1}^{4}\left[e^{\frac{r_0 - r_i}{0.37}} \left(1 - 3\cos^2\theta_i\right)\log D \Big/ R_i^3 \right], \tag{2}$$

and the angles and distances, θ, r, R and D are as shown in Figure 1c and r_0 is the length of the bond of unit valence (tabulated by Brown and Altermatt,[27] except for Si and Al, for which the respective values of 1.64 and 1.62 Å were re-determined by Sherriff *et al.*[26]), provided a reasonable prediction of δ_{iso}, reported for a range of Si-containing motifs in minerals (giving a root mean squared deviation of 0.66 ppm over 60 silicates).

A major source of possible error in all of the relationships discussed above is that they often seek to compare experimental crystallographic data with experimental NMR spectra. While this is, of course, the ultimate aim of these relationships: to be able to determine structural parameters from an NMR spectrum (or to predict an NMR spectrum from an experimental structure), the techniques are sensitive to structure on very different lengthscales. As an example, the "Si–O" bonds reported for an aluminosilicate typically (unless the Al is well ordered) represent the weighted mean Si-O and Al-O bond lengths (typically ~1.6 and 1.7 Å, respectively), whereas the ^{29}Si NMR spectrum will be sensitive to only the Si–O bond lengths. With some of the relationships mentioned above reporting a variation in chemical shift of ~1000 ppm per Å, a 1 pm error in bond length can have an effect similar to substitution of a neighbouring Si for Al (*cf.* ~10 ppm per pm and ~7 ppm

per Al). While this may be a somewhat extreme example (or may, in fact, suggest that the substitution of a single Al leads to an increase in $\langle r_{SiO} \rangle$ of ~1 pm), other smaller errors relating to temperature effects are also relevant, with magic angle spinning (MAS) NMR spectra typically recorded at just above room temperature whereas crystal structures are typically obtained at lower temperature where thermal motion is reduced. Therefore, in order to determine whether there is any true worth in attempting to relate simple geometric parameters such as mean bond lengths and angles to the experimental NMR spectrum, in this work we compare the NMR parameters calculated for exactly known model systems (small clusters and extended zeolite-like solids), where the experimental errors in both structure and chemical shift referencing are removed.

The use of empirical structure-spectrum relationships has largely been superseded by the use of quantum-chemical calculations, most notably using density functional theory (DFT). Periodic planewave DFT approaches have made highly-accurate calculations of NMR parameters of extended periodic solids almost a routine accompaniment to solid-state NMR spectroscopy.[28-31] At their most basic, the calculations can confirm an assignment, but the ease with which a structural model can be manipulated, perhaps to investigate cation or anion substitution or motion, means that these calculations provide extremely detailed insight into a range of challenging systems that exhibit complex spectra arising from non-periodic features.[32,33] However, there remain systems where it is too costly to apply DFT calculations of NMR parameters, most notably in molecular dynamics calculations, where the simulation of just a few ps of motion can lead to a "trajectory" comprising many thousands of structural snapshots. Applying DFT calculations to all of these would rapidly lead to computational costs on the order of CPU decades, which is unfortunate, since it is the dynamic processes occurring within many materials, including zeolites, that are of most interest to their applications and NMR should be ideally placed to study these, owing to its sensitivity both to local structure and motion spanning ~12 orders of magnitude.[33,34] Therefore, in order to provide a bridge between structures and materials where NMR spectra are likely to be of most interest and DFT calculations would prove too costly, we attempt here to determine whether there are any underlying

structure-spectrum relationships that can be used to predict NMR parameters with near DFT-level accuracy, without invoking costly computation.

Building on our earlier work on calcined aluminophosphates (AlPOs),[35] in this work we consider the effect of various local structural parameters on the ^{29}Si δ_{iso} for a series of simple model clusters and zeolitic SiO_2 frameworks. We show that, by considering multiple geometrical parameters simultaneously, a more robust relationship between spectra and structural parameters can be obtained. Ultimately, we hope that the relationship we have determined will find application in more disordered materials, or in molecular dynamics simulations, where it may not be feasible to calculate NMR parameters using relatively costly DFT methods.

Computational Details

DFT Calculations

Model cluster DFT calculations were carried out using Gaussian 03 (revision D.01)[36] using the continuous set of gauge transformations (CSGT) method to calculate the NMR parameters. The B3LYP hybrid GGA functional was used, with the 6-311+G(d,p) basis set employed for H and O, and the aug-pcS-2 basis set (which has been optimised to provide accurate nuclear magnetic shielding parameters)[37] for Si. Prior to the calculation of the NMR parameters, the structures of the clusters were optimized to an energy minimum, with the parameters specified in the text constrained to their stated values. Calculations were carried out using either a local cluster comprising four Intel Core i7−930 quad-core processors with 6 GB memory per core or the EaStCHEM Research Computing Facility, comprising a 198-node (2376-core) Intel Westmere cluster with 2 GB memory per core and QDR Infiniband interconnects.

Periodic DFT calculations were performed using version 16.11 of the planewave CASTEP code,[38] which employs the GIPAW algorithm[39] to reconstruct the all-electron wavefunction in the presence of a magnetic field. The generalized gradient approximation

(GGA) PBE[40] functional was employed, and core−valence interactions were described by ultrasoft pseudopotentials,[41] which were generated on the fly. Wavefunctions were expanded as planewaves with a kinetic energy smaller than a cutoff energy of 60 Ry (816 eV). Integrals over the first Brillouin zone were performed using a Monkhorst−Pack grid with a k-point spacing of 0.04 2π Å^{-1}. Where optimisation of the structure to an energy minimum was carried out, this used the same cutoff energy and k-point spacing as above, and with all atomic coordinates and unit cell parameters allowed to vary. Calculations were performed using the EaStCHEM Research Computing Facility, comprising a 54-node (1728-core) Intel Broadwell cluster with 4 GB memory per core and FDR Infiniband interconnects at the University of St Andrews.

Calculations generate the absolute shielding tensor, $\boldsymbol{\sigma}$, in the crystal frame. From the principal components of the symmetric part of $\boldsymbol{\sigma}$ it is possible to generate the isotropic shielding, $\sigma_{iso} = (1/3) \, Tr\{\boldsymbol{\sigma}\}$. The isotropic chemical shift is given (assuming $\sigma_{ref} \ll 1$) by $\delta_{iso} = -(\sigma_{iso} - \sigma_{ref})/m$, where σ_{ref} is a reference shielding, here (for the CASTEP calculations) 289.13 ppm for ^{29}Si and m is a scaling factor, ideally 1 but, here, 1.3652. The values for σ_{ref} and m were determined by comparing experimental and calculated chemical shifts for MFI- and FER-type SiO_2.[42,43]

Linear Regression

Multivariate linear regression was carried out using the MATLAB[44] routines described in the Supporting Information (S1). All values generated by MATLAB are truncated to 5 significant figures.

Results and Discussion

Model Cluster Calculations

Using an approach shown earlier to be successful for AlPOs,[35] the influence of $\langle \theta_{SiOSi} \rangle$ and $\langle r_{SiO} \rangle$ on the calculated ^{29}Si σ_{iso} was investigated using several series of model $Si(OSi(OH)_3)_4$ clusters, shown in Figure 2a. These clusters allow systematic (and

independent) variation of $\langle\theta_{SiOSi}\rangle$ and $\langle r_{SiO}\rangle$ for the central Si, without considering the longer-range effects of an extended zeolitic framework. For investigations into the effect of $\langle\theta_{SiOSi}\rangle$, the central SiO_4 tetrahedron was fixed with the ideal Si–O length of 1.62 Å and O-SiO angles of 109.47°, while $\langle\theta_{SiOSi}\rangle$ was varied according to Table 1. When only $\langle\theta_{SiOSi}\rangle$ is varied (series 1), there is a strong linear correlation (R^2 = 0.972) between σ_{iso} and $\langle\theta_{SiOSi}\rangle$, with a gradient of 1.04 ppm per degree, which is remarkably similar to that found previously for ^{31}P in AlPOs (1.05 ppm per degree variation in $\langle\theta_{POAl}\rangle$).[35] However, as also observed earlier, there is some deviation from this straight line as the angle approaches 180°. The relationship

$$\sigma_{iso} = 353.61 - 113.21\cos\left(\langle\theta_{SiOSi}\rangle\right), \tag{3}$$

(where the stated coefficients give σ_{iso} in ppm) provides an improved correlation coefficient (R^2 = 0.9988) and, crucially, the deviation from the straight line is now less dependent on the angle. The term $\cos(\langle\theta_{SiOSi}\rangle)/[\cos(\langle\theta_{SiOSi}\rangle)-1]$[23] gave a poorer value of R^2 (0.9844) and was not considered further. Figures 2b and c shows plots of [29]Si σ_{iso} against $\cos(\langle\theta_{SiOSi}\rangle)$ and the standard deviation of θ_{SiOSi}, $\sigma(\theta_{SiOSi})$, for series 1-8. In series 2-6, $\langle\theta_{SiOSi}\rangle$ was kept constant at 140° while $\sigma(\theta_{SiOSi})$ was varied as indicated in Table 1. As can be seen from the inset in Figure 2b, a difference is observed of up to −6.8 ppm (series 3, n = 5) in σ_{iso} relative to the corresponding point of series 1 (n = 4), in which $\langle\theta_{SiOSi}\rangle$ = 140° and $\sigma(\theta_{SiOSi})$ = 0. This is similar to our earlier observation for AlPOs that the individual bond angles contribute to [31]P σ_{iso}, rather than simply the mean bond angle. Series 7, where both $\langle\theta_{SiOSi}\rangle$ and $\sigma(\theta_{SiOSi})$ were varied systematically (see Table 1) provides further evidence that the individual θ_{SiOSi}, rather than just $\langle\theta_{SiOSi}\rangle$, are of importance. As can be seen from Figure 2b, there is a strong linear relationship between σ_{iso} and $\cos(\langle\theta_{SiOSi}\rangle)$, with

$$\sigma_{iso} = 326.49 - 99.41\cos\left(\langle\theta_{SiOSi}\rangle\right), \tag{4}$$

although there is significant deviation from linearity towards lower $\cos(\langle\theta_{SiOSi}\rangle)$ (higher $\sigma(\theta_{SiOSi})$). To further investigate the contributions of $\langle\theta_{SiOSi}\rangle$ and $\sigma(\theta_{SiOSi})$, in series 8 the bond angles were all randomly generated (see the Supporting Information (S2) for values). From Figure 2b, it can be seen that series 1 and 8 have a very similar relationship between

σ_{iso} and $\cos(\langle\theta_{SiOSi}\rangle)$, with series 8 described by

$$\sigma_{iso} = 360.30 - 100.52\cos\left(\langle\theta_{SiOSi}\rangle\right). \tag{5}$$

This similarity to Equation 3, suggests that $\cos(\langle\theta_{SiOSi}\rangle)$ is a reasonably good predictor of σ_{iso}, although, clearly, the variation in individual bond angles leads to some scatter in the shielding for a given mean bond angle (R^2 for series 8 is 0.9738 and the mean absolute error (MAE) in σ_{iso} calculated by DFT and from Equation 5 is 1.01 ppm). Using multivariate linear regression (see the Supporting Information (S1) for more details), the contributions of both $\cos(\langle\theta_{SiOSi}\rangle)$ and $\sigma(\theta_{SiOSi})$ to σ_{iso} can be determined, with

$$\sigma_{iso} = 362.24 - 103.08\cos\left(\langle\theta_{SiOSi}\rangle\right) - 0.22668\,\sigma(\theta_{SiOSi}), \tag{6}$$

which increases R^2 to 0.9966 and reduces the MAE to 0.38 ppm for series 8.

As discussed above, many attempts have also been made to link σ_{iso} with the mean Si–O bond length, $\langle r_{SiO}\rangle$.[3,6-12] This was investigated using a second set of model clusters, where all O−Si−O and Si−O−Si bond angles were constrained to 109.47 and 140°, respectively, and $\langle r_{SiO}\rangle$ was varied systematically as given in Table 2. It can be seen from Figure 3 that when only $\langle r_{SiO}\rangle$ is allowed to vary and all other structural parameters are kept constant (series 9), σ_{iso} and $\langle r_{SiO}\rangle$ are related by the quadratic function

$$\sigma_{iso} = -547.68\,\langle r_{SiO}\rangle^2 + 1799.7\,\langle r_{SiO}\rangle - 1038.8, \tag{7}$$

with R^2 = 0.9995. This is similar to our previous finding for ^{31}P in calcined AlPOs.[35] In series 10 and 11 the value of $\langle r_{SiO}\rangle$ was fixed at 1.62 Å, while the standard deviation in the Si-O bond lengths, $\sigma(r_{SiO})$, was systematically varied (see Table 2). This resulted in differences of up to −1.4 ppm (series 11, n = 6) in σ_{iso} relative to the corresponding point of series 9 (n = 0), in which $\sigma(r_{SiO})$ = 0. As above for the Si–O–Si bond angles, this suggests that the [29]Si σ_{iso} is sensitive to the individual Si–O bond lengths, rather than just their average value. In series 12 both $\langle r_{SiO}\rangle$ and $\sigma(r_{SiO})$ were varied systematically (see Table 2) and, as can be seen from Figure 3a, the σ_{iso} values for this series are in reasonably good agreement with Equation 7, although it must be noted that the range of $\sigma(r_{SiO})$ for series 12

is relatively small compared to those for series 10 and 11, where larger deviations from Equation 7 are observed. In series 13, all Si–O bond lengths were randomly generated between 1.45 and 1.85 (see the Supporting Information (S2) for details), giving a maximum $\sigma(r_{SiO})$ of 0.14 Å. From Figure 3a, it can be seen that the data from series 13 describe a very rough parabola, with the best-fit quadratic function,

$$\sigma_{iso} = -480.00 \langle r_{SiO} \rangle^2 + 1590.3 \langle r_{SiO} \rangle - 880.07 \,, \tag{8}$$

with a correlation coefficient of $R^2 = 0.84$. Using multivariate linear regression, it is possible to account for variation in both $\langle r_{SiO} \rangle$ and $\sigma(r_{SiO})$, with

$$\sigma_{iso} = -547.72 \langle r_{SiO} \rangle^2 + 1812.8 \langle r_{SiO} \rangle - 39.071 \, \sigma(r_{SiO}) - 1059.0 \,, \tag{9}$$

which is very close to Equation 7 (in the limit of $\sigma(r_{SiO}) = 0$) and improves R^2 to 0.98 for series 13.

Model SiO$_2$ Frameworks

From the model cluster calculations it can be seen that both the mean Si–O–Si bond angles and Si-O bond lengths, as well as the standard deviations in their values, influence the ^{29}Si σ_{iso}, which goes some way to explaining why many of the relationships between a single structural parameter and ^{29}Si chemical shift in the literature disagree to some extent and are not generally transferrable. To investigate whether these findings are relevant in the extended periodic structures of zeolites, where variation in all of these parameters may occur simultaneously and independently, calculations were carried out on a series of model zeolitic SiO$_2$ polymorphs using the periodic planewave code, CASTEP.[38] There is, of course, a large and well-documented effect on the ^{29}Si δ_{iso} as the number of next-nearest neighbour Si species is changed, either as a function of condensation (*e.g.*, Q^2 Si(OSi)$_2$(OH)$_2$ *vs.* Q^{4}Si(OSi)$_4$ species) or as a function of cation substitution (*e.g.*, Q^{4}Si(OSi)$_4$ *vs.* Q^{4}Si(OSi)$_3$(OAl) species)[3,4] and so, to avoid complications arising from this, structures taken from the literature (with international zeolite association framework topology codes[45] of EDI, ITG, JBW, MTT, SFE, THO and VET – see the Supporting Information (S3) for further details) were converted to idealised models where all framework "T" atoms

were 100% occupied by Si. This also provided a charge-neutral framework that allowed for removal of the extraframework cations and H_2O within the pores, leading to a set of 7 microporous SiO_2 structures containing 49 crystallographically-unique Si atoms. The structure of the dense phase α-quartz, containing one unique Si site, was also included. NMR parameters were calculated for these structures before and after optimisation to an energy minimum, leading to the consideration of 100 unique Si atoms. As discussed below, the structures showed significantly greater variation in the Si–O bond lengths and O-Si-O bond angles prior to optimisation, so all structures were considered here in order to ensure that the study was as widely applicable as possible to the various types of structures that may be encountered in real materials of interest.

Figures 4a and b plot the calculated [29]Si δ_{iso} for the set of 16 structures (*i.e.*, prior to and post optimisation) against $\cos(\langle\theta_{SiOSi}\rangle)$ and $\langle r_{SiO}\rangle$, respectively, and it can be seen that there is a strong linear correlation with $\cos(\langle\theta_{SiOSi}\rangle)$,

$$\delta_{iso} = 79.863\cos(\langle\theta_{SiOSi}\rangle) - 42.823 \ , \tag{10}$$

but a less apparent correlation with $\langle r_{SiO}\rangle$ for the "real" data. While the dependence on $\cos(\langle\theta_{SiOSi}\rangle)$ is similar to that in Equations 3 and 5 (note the change in sign arises from changing from σ_{iso} to δ_{iso}), there is still some scatter ($R^2 = 0.89$) and the MAE is 1.23 ppm, which is insufficient to provide a generally useful link between an NMR spectrum and a given structure. As described in the Supporting Information (S1), multivariate linear regression was used to generate a relationship dependent on multiple structural parameters, giving

$$\delta_{iso} = 11.531\langle r_{SiO}\rangle + 27.280\,\sigma(r_{SiO}) + 83.730\cos(\langle\theta_{SiOSi}\rangle) + 0.20246\,\sigma(\theta_{SiOSi}) - 59.999 \ , \tag{11}$$

where, as noted in the Supporting Information (S1), the $\langle r_{SiO}\rangle^2$ term was discarded as this is effectively collinear with $\langle r_{SiO}\rangle$ over the relevant range of Si–O bond lengths (see below). Equation 11 can be seen to contain coefficients whose magnitudes (accounting again for the change in sign from σ_{iso} to δ_{iso}) are very similar to those found in Equations 3, 6 and 9 (for $\cos(\langle\theta_{SiOSi}\rangle)$, $\sigma(\theta_{SiOSi})$ and $\sigma(r_{SiO})$, respectively), with the degree of similarity especially

surprising given that the earlier equations relate to calculations for very simple model systems carried out using a completely different code and level of theory. Figure 4(c) shows a plot of ^{29}Si σ_{iso} calculated using CASTEP against that from Equation 11. It can be seen that there is excellent agreement, with R^2 now increased to 0.945 and the MAE reduced to 0.97 ppm. The MAE is now affected mainly by the unoptimised MTT structure, which contains unusually short $\langle r_{SiO} \rangle$ (1.568-1.594 Å) and the "Al" sites of unoptimised JBW and THO, which have unusually long $\langle r_{SiO} \rangle$ (1.675-1.749 Å), leading to a discrepancy between CASTEP and Equation 11 of up to 4.9 ppm for very short bonds and 4.4 ppm for very long bonds. It could, therefore, be suggested that a quadratic dependence on $\langle r_{SiO} \rangle$ may be required to make the structure-spectrum relationship more generally useful. However, as discussed below, it is unlikely that such extremes of Si-O bond lengths would be observed in real SiO_2 zeolites.

To gain some insight into the errors in the coefficients in Equation 11, the structure-spectrum relationship was re-calculated for each of the 12870 unique combinations of 8 structures selected from the 16 considered here (see the Supporting Information (S1) for details). Histograms showing the distribution of coefficients determined this way are shown in Figure 5 and it can be seen that, when only 8 structures are considered, there is significant uncertainty in many of these values, depending on the structure set chosen. However, as shown in the Supporting Information (S4), the distributions of coefficients are essentially independent of one another, with the exception of the coefficient for $\langle r_{SiO} \rangle$, which is strongly correlated with the intercept ($R^2 = 0.9929$), so that it remains unclear to what extent this structural parameter actually influences δ_{iso}. As discussed above, this may result from the approximation that ^{29}Si δ_{iso} depends only linearly on $\langle r_{SiO} \rangle$, leading to sets including one or more structures with unusually long or short Si–O bonds contributing to spurious values of the coefficient. We do not, however, observe any coefficients for $\langle r_{SiO} \rangle$ approaching the ~1000 ppm Å^{-1} mentioned in the introduction. This significant variation goes some way to explaining the distribution of relationships within the literature, where, depending on the subset of zeolites chosen, it would be possible to obtain very disparate structure-spectrum relationships. It is particularly worthy of note that 10% of the

relationships determined found no dependence on $\langle r_{SiO} \rangle$, whereas the coefficients for $\cos(\langle \theta_{SiOSi} \rangle)$ were always non-zero and very similar, suggesting that the contribution from $\langle \theta_{SiOSi} \rangle$ to δ_{iso} is more universally applicable.

It is worth comparing the results of Equation 11 to the relationship of Sherriff *et al.*,[26] that was also reported to be universal and parameterised using (experimental) data for a wide range of structure types. As discussed in the Supporting Information (S5), for the test set of SiO_2 frameworks discussed above there is significant scatter from the ideal 1 : –1 correspondence expected. However, the Sherriff model performs remarkably well for the optimised structures ($R^2 = 0.96$) and very poorly for the unoptimised structures ($R^2 = 0.50$), indicating it may suffer from some overparameterisation and be less applicable to either more unusually distorted frameworks (see below) than our own model, which was parameterised using a set of structures that included some with more extreme distortions.

Structural Changes upon Optimisation

As discussed above, there is some indication that at the extremes of $\langle r_{SiO} \rangle$ there may be a quadratic relationship between this term and σ_{iso}. However, upon optimisation of the eight structures considered here, it was observed that the individual Si-O bonds all fall within the range of 1.603 to 1.643 Å (see Figure 6a), indicating that the very long and short bonds observed for the unoptimized structures above arise from the fact that these were derived from experimental structures for (alumino)silicates containing guest cations and water molecules within the pores. The optimum value of r_{SiO} observed here is in good agreement with the mean value of 1.597(26) Å reported by Wragg *et al.*[46] in a study of 35 experimental zeolite structures (although, since these structures were not optimized, a range from 1.54 to 1.67 Å was observed for individual bond lengths), with the slight increase observed in the DFT calculations possibly arising from thermal motion of the O atoms[47] (since the structures in the DFT calculations were effectively at 0 K whereas the experimental structures were obtained at finite temperature). In pure calcined SiO_2 polymorphs, then, such a variation in bond lengths is much less likely. However, while the bond lengths of the SiO_4 tetrahedra tended towards all being equal, the O–Si–O bond

angles did not necessarily optimise to closer to the ideal tetrahedral angle, $\theta_0 = 109.471°$ but, rather, the distortion index,

$$\text{DI} = \frac{\sum_i |\theta_i - \theta_0|}{6}, \tag{12}$$

tended to fall within the range of DI ≤ 2.0°, as shown in Figure 6b (the point on the dotted grey line indicating DI = 2.0° is Si3 of the VET structure, for which DI changed from 3.312° to 1.991° on optimisation). When DI was very small in the initial structure, optimisation often led to an increase, but never above the threshold of 2°. There is no optimum value of θ_{SiOSi}, as shown in Figure 6c, since this parameter is strongly dictated by the framework topology.[46] These observations suggest that, at least for pure silicates, the values of $\langle r_{SiO} \rangle$ and DI might be used as an indicator for an unrealistic structure. However, the situation becomes more complicated when considering, for example, an aluminosilicate with fractional occupancy of Si sites by Al, which has longer bonds to O and may also be higher coordinate, leading to a superposition of several contributions to the final "SiO$_4$" tetrahedron in the crystal structure, and a wider distribution of $\langle r_{SiO} \rangle$ and DI might be expected for (disordered) substituted frameworks. Such experimental crystal structures will not, of course, represent accurate representations of the true local geometry, even if they are correct for the long-range average structures.

Applications to Siliceous Zeolites

There are many examples of pure SiO_2 zeolites in the literature, where the combination of detailed ^{29}Si homonuclear correlation NMR spectroscopy, high-quality crystallographic data and, in some cases, DFT calculations, have been used to provide a full spectral assignment.[2] Here, we provide two examples to demonstrate the ability of Equation 11 to help provide both spectral assignment based on the crystal structure and structural validation based on the NMR spectrum.

The structure of the monoclinic form of MFI-type SiO_2 ZSM-5 was determined by van Konningsfeld *et al.*[48] and contains 24 crystallographically-distinct Si species with $\langle r_{SiO} \rangle$ and $\langle \theta_{SiOSi} \rangle$ covering the relatively narrow ranges of 1.589-1.601 Å and 147.11-158.83°,

respectively. From the ^{29}Si NMR spectrum of the material, Fyfe *et al.*[42] were able to resolve and assign 16 resonances or groups of resonances (within a shift window of only ~7 ppm) based on homonuclear ^{29}Si double-quantum correlation spectra. Figure 7 plots the ^{29}Si chemical shifts predicted from Equation 11 (using the structure of van Konnigsveld *et al.*) against the corresponding experimental values. There is good agreement in the order of the shifts, although the predicted values have an overall spread of ~8 ppm and an offset of ~1.2 ppm. Figure 7 also shows the ^{29}Si chemical shifts calculated by DFT (again using the structure of van Konnigsveld *et al.* without optimisation), and the agreement between calculation and experiment is very good. This example demonstrates that, when a high-quality crystal structure is available, Equation 11 can be used to provide at least an initial assignment, even when the structure contains many distinct Si sites.

Morris *et al.* determined the structure of siliceous ferrierite (FER topology) and recorded high-resolution one- and two-dimensional ^{29}Si NMR spectra of the material.[43] Five resonances were observed, corresponding to the five crystallographic Si sites, and these could be partially assigned using double-quantum correlation spectroscopy. The final two sites, Si4 and Si5 were assigned based on a correlation between δ_{iso} and $\cos(\langle\theta_{SiOSi}\rangle)/\cos(\langle\theta_{SiOSi}\rangle)-1$. The filled circles in Figure 8 show the ^{29}Si δ_{iso} predicted by Equation 11 for the experimental structure of silica ferrierite. The experimental points (shown by crosses in Figure 8) cover a smaller shift range than predicted and agreement with calculation is poor. On closer inspection, the experimentally-determined structure of is likely to be unrealistic, with DI > 2.0 for four of the five Si sites. Morris *et al.* also optimised the structure using a forcefield method, leading to DI < 2.0 for four of the five Si sites. Despite this optimisation, the MAE in the shifts predicted by Equation 11 (not shown) actually increases from 1.19 ppm for the experimental structure to 1.27 ppm after optimisation. The open circles in Figure 8 represent δ_{iso} calculated by CASTEP for the experimental structure and it can be seen that Equation 11 predicts these well, even though agreement with the experimental shifts is poor. This confirms that the structures are likely to be unrealistic, rather than that Equation 11 cannot predict the values obtained by DFT. Upon optimisation of the structure using CASTEP, the DI is reduced to below 1.5°

for all five Si sites. From this optimised structure, CASTEP calculates values of δ_{iso} in excellent agreement with experiment (open squares in Figure 8) and Equation 11 predicts very similar values (filled squares in Figure 8), with a MAE of just 0.82 ppm (*cf.* the 0.92 ppm for the CASTEP values), although the order of the shifts for Si1 and Si5 is reversed. This example demonstrates that, even where a structure is an unrealistic representation of the material, Equation 11 is able to rapidly predict the outcome of the DFT calculation and, therefore, any large discrepancies between the experimental and predicted δ_{iso} most likely indicate that the structure must be improved.

Re-Examining the Literature Data

Using Equation 11, it is possible to predict δ_{iso} from the crystallographic structures of the tectosilicates for which spectral data[7,8,14-16,19] was shown in Figure 1. Note that data for other classes of silicates were not considered here, as these contain Si with lower degrees of condensation. Where possible, the experimental crystallographic structures referenced in the original spectroscopic studies[48-72] were used here (see the Supporting Information (S6) for further details). Figure 9a shows a plot of the reported experimental ^{29}Si δ_{iso} against that predicted by Equation 11 for all 31 tectosilicates (78 Si sites) discussed above. The points all lie reasonably close to the ideal line of 1:1 correspondence, although there is significant scatter, with a MAE of 4.7 ppm and a maximum deviation of 22.1 ppm. However, the greatest deviations are for the data reported by Newsam[15] (highlighted in red in the figure), which is unsurprising, since the experimental data were reported for $Si(OAl)_4$ resonances, whereas Equation 11 inherently assumes $Si(OSi)_4$ species. Figure 9b shows that, when these points are not included in the plot, much better agreement is now obtained, with a MAE of 2.5 ppm and a maximum deviation of 11.3 ppm. As demonstrated above, at least for pure silicate zeolites, structures or sites with DI > 2.0° are unlikely to represent an energetic minimum and can, therefore, be considered poor descriptions of the true structure (for whatever practical reason). In the present data set, there are 15 SiO_4 tetrahedra with DI > 2.0° (highlighted in blue in Figures 9a and 9b) and, when these are also removed from the plot, as shown in Figure 9c, the MAE drops to 1.5 ppm and the maximum deviation is now 6.2 ppm. While this MAE may not appear to be

particularly low (certainly not within the < 1 ppm accuracy required for interpreting some [29]Si spectra of zeolites, as in the examples above), it is actually surprisingly small, given that the experimental structures include those determined for aluminosilicates where (in several cases) the Al sites in the framework were not located and the cations and water molecules in the pores (where present) were not considered in the chemical shift prediction. Furthermore, the structures were not optimised to an energy minimum (as would be carried out when the DFT-based prediction of accurate NMR parameters would be required[13,73]) and there are several cases of small (~1 ppm) discrepancies between [29]Si δ_{iso} values reported for the same Si site in the same material by different authors. Given the number of accumulated experimental errors present in the dataset it is, in fact, more remarkable that such a simple structure-spectrum relationship as Equation 11 can predict the experimental results so closely.

The prediction of [29]Si δ_{iso} from experimental crystal structures that may contain disordered framework substitution, extraframework cations or water suggests that one such application of the work considered here might be in understanding the NMR spectra of real zeolites, where the disorder is too great to allow the application of meaningful DFT calculations. In such cases, the spectral resonances are generally broadened by this disorder and predicting isotropic shifts to < 1 ppm accuracy is probably not required.

Conclusions

The use of empirical structure-spectrum relationships between [29]Si δ_{iso} and the local bonding geometry around Si in zeolites is an area that has received intense interest from the 1970s until the beginning of the 21st century, when computing methods and hardware became sufficiently powerful to predict accurate NMR spectra from extended periodic crystal structures. However, there remain many structures and questions that DFT calculations are (currently at least) ill suited to handle – for example, where low amounts of Al occupies the tetrahedral sites in a zeolite, a series of large "supercell" calculations may be required to accurately model the distribution of Al ions within the material. In

addition, atoms and molecular species such as Brønsted acidic H, water and disordered (or dynamic) SDA cations may not be located (or, indeed, locatable) by diffraction experiments. In the most interesting case of modelling catalytic processes occurring within zeolites using molecular dynamics, there is a need to be able to provide a link between the thousands of structures generated per MD trajectory and experimental measurements including *in situ* NMR spectroscopy, which can (at least in principle) provide a rich variety of information on chemical species present, their concentrations and any dynamics that may be present. In all of these cases, the need to be able to calculate NMR parameters to DFT-level accuracy is clear, but it is also evident that such calculations would be very time consuming and not necessarily possible on routinely available computing hardware. In light of this, we re-examined the early empirical work that compared experimental NMR parameters with experimental structures (complete with experimental errors in both sets of data), using DFT calculations and more detailed statistical analysis to determine whether it is, indeed, possible to relate the local bonding geometry to the NMR spectrum in a simple way, or whether the disparate relationships reported in the literature were merely the result of chance fluctuations in the structures of the relatively small numbers of zeolites studied in any one case.

DFT calculations were first carried out on small $Si(OSi(OH)_3)_4$ clusters to model the immediate bonding environment around Si in a SiO_2 zeolite. These clusters allowed ready systematic manipulation of the bonding geometry and revealed that both the mean Si–O bond length and the mean Si-O-Si bond angle have a strong influence on ^{29}Si δ_{iso}. It was also clear from these calculations that the standard deviations of Si-O bond lengths and Si–O–Si bond angles influence δ_{iso}, but to a lesser degree compared to the mean values. This approach was then applied to more realistic model microporous SiO_2 frameworks, to investigate whether there were any additional longer-range effects arising from the extended periodic structure. We demonstrated that the relationships determined for the model clusters could be applied almost directly to the periodic frameworks, although the quadratic relationship between the mean Si–O bond length and δ_{iso} observed for the cluster compounds was revised to a simple linear relationship as, over the relevant range

of bond lengths (*i.e.*, 1.55 to 1.75 Å), x and x^2 are essentially collinear. The final structure-spectrum relationship allowed the prediction to within ~1 ppm of δ_{iso} calculated from DFT-level calculations with only knowledge of the Si–O bond lengths and Si-O-Si bond angles. The relationship was tested first on MFI- and FER-type SiO_2 frameworks, and was able to match the order of the experimentally-determined spectral assignment for many of the 24 Si sites in the MFI framework, allowing at least a preliminary assignment. Agreement with experiment was poorer for the FER-type material, but improved to within 0.82 ppm upon structural optimisation with DFT. These results demonstrate that our structure-spectrum relationship can accurately predict the DFT-calculated NMR parameters and, where significant disagreement is observed with the experimental spectrum, this may indicate that the crystal structure requires optimisation. The relationship was also tested on published experimental crystal structures and NMR spectroscopic data for a range of tectosilicates and was able to predict the experimental δ_{iso} for $Si(OSi)_4$ species to within 1.5 ppm (on average). However, the error was larger for $Si(OAl)_4$ species owing to the known relationship between ^{29}Si δ_{iso} and next-nearest neighbour Al/Si substitution. Our relationship was parameterised for SiO_2 zeolites only and will require modification to take into account other cation substitutions.

To determine whether a given crystal structure represents a realistic energy minimum, the geometries of the set of model tectosilicates were optimised. This showed that the mean Si–O bond lengths converge to ~1.62 Å and the distortion index is always below 2.0° for optimised structures. There was, however, no optimum value for the Si–O–Si angles. In other words, the SiO_4 tetrahedron will be as close to ideal as possible (to within some tolerance dictated by crystal symmetry and framework topology), whereas the geometry of the connections between the tetrahedra (Si–O–Si linkages) is dictated by the long-range topology of the framework. By removing unrealistic SiO_4 tetrahedra from the set of experimental structures and chemical shifts, the accuracy of the predictions was improved to 2.0 ppm, which is remarkable given the number of potential experimental errors in the structures and NMR data, and also the simplicity of the structural model used for the predictions.

This approach will never supersede DFT calculations, where such are possible. However, we envisage that the ability to predict shifts with close to DFT-level accuracy for systems where DFT is impractical or impossible will be a great advantage in providing a stronger link between experimental NMR spectroscopic measurements and structural and mechanistic models for a wide variety of experimental and computational studies.

Acknowledgements

Supporting Information: Supporting information includes a description of the linear regression methods, the generation of bond lengths and angles for clusters, a description of the idealised zeolite model used, analysis of the relation of the coefficients used, a comparison to the Sherriff Model and references for the spectroscopic and structural data used.

References

1. Wright, P. A. *Microporous Framework Solids*, **2008**, Royal Society of Chemistry, Cambridge, UK.

2. Ashbrook, S. E.; Dawson, D. M.; Seymour, V. R. Recent Developments in Solid-State NMR Spectroscopy of Crystalline Microporous Materials. *Phys. Chem. Chem. Phys.* **2014**, *16*, 8223-8242.

3. MacKenzie, K. J. D.; Smith, M. E. *Multinuclear Solid-State Nuclear Magnetic Resonance of Inorganic Materials*, **2002**, Elsevier Science Ltd, Oxford, UK.

4. Lippmaa, E.; Mägi M.; Samoson, A.; Engelhardt, G.; Grimmer, A.-R. Structural Studies of Silicates by Solid-State High-Resolution ^{29}Si NMR. *J. Am. Chem. Soc.* **1980**, *102*, 4889-4893.

5. Brouwer, D. H.; Darton, R. J.; Morris, R. E.; Levitt, M. H. A Solid-State NMR Method for Solution of Zeolite Crystal Structures. *J. Am. Chem. Soc.* **2005**, *127*, 10365-10370.

6. Smith, K. A.; Kirkpatrick, R. J.; Oldfield, E.; Henderson, D. M. High-Resolution Silicon-29 Nuclear Magnetic Resonance Spectroscopic Study of Rock-Forming Silicates. *Am. Mineral.* **1983**, *68*, 1206-1215.

7. Smith, J. V.; Blackwell, C. S. Nuclear Magnetic Resonance of Silica Polymorphs. *Nature* **1983**, *303*, 223-225.

8. Smith, J. V.; Blackwell, C. S.; Hovis, G. L. NMR of Albite-Microcline Series. *Nature* **1984**, *09*, 140-142.

9. Grimmer, A. R. Correlation between Individual Si-O Bond Lengths and the Principal Values of the ^{29}Si Chemical Shift Tensor in Solid Silicates. *Chem. Phys. Lett.* **1985**, *119*, 416-420.

10. Higgins, J. B.; Woessner, D. E. ^{19}Si, ^{27}Al and ^{23}Na NMR Spectra of Framework Silicates. *EOS*, **1982**, *63*, 1139-1167.

11. Grimmer A. R.; Radeglia, R. Correlation between the Isotropic ^{29}Si Chemical Shifts and the Mean Silicon-Oxygen Bond Lengths in Silicates. *Chem. Phys. Lett.* **1984**, *106*, 262-265.

12. Weiden, N.; Rager, H. The Chemical Shift of the ^{29}Si Nuclear Magnetic Resonance in a Synthetic Single Crystal of Mg_2SiO_4. *Z. Naturforsch.* **1985**, *40A*, 126-130.

13. Hochgräfe , M.; Gies, H.; Fyfe, C. A.; Feng, Y.; Grodney, H. Lattice Energy-Minimization Calculation in the Further Investigation of XRD and NMR Studies of Zeolite Frameworks. *Chem. Mater.*, **2000**, *12*, 336-342.

14. Engelhardt, G.; Radeglia, R. A Semi-Empirical Quantum-Chemical Rationalization of the Correlation between SiOSi Angles and ^{29}Si NMR Chemical Shifts of Silica Polymorphs and Framework Aluminosilicates (Zeolites). *Chem. Phys. Lett.* **1984**, *108*, 271-274.

15. Newsam, J. M. Silicon-29 Chemical Shifts in Sodalite Materials. *J. Phys. Chem.* **1987**, *91*, 1259-1262.

16. Thomas, J. M.; Klinowski, J.; Ramdas, S.; Hunter, B. K.; Tennakoon, D. T. B. The Evaluation of Non-Equivalent Tetrahedral Sites from ^{29}Si NMR Chemical Shifts In Zeolites and Related Aluminosilicates. *Chem. Phys. Lett.* **1983**, *102*, 158-162.

17. Mortuza M. G.; Dupree, R.; Holland, D. Devitrification of Sodium Disilicate Glass: a NMR Study. *J. Mater. Sci.* **1998**, *33*, 3737-3740.

18. Jarman, R. H. [29] Si N.M.R. Study of High Silica Tetramethylammonium-Sodalite. *J. Chem. Soc., Chem. Commun.* **1983**, 512-513.

19. Sivadinarayana, C.; Choudhary, V. R.; Vetrivel, R.; Ganapathy, S. Characterization of Silicon Sites in Monoclinic Zeolite ZSM-5 Using [29]Si Magic Angle Spinning (MAS) Nuclear Magnetic Resonance (NMR) and Molecular Modelling. *Solid State Nucl. Magn. Reson.* **1998**, *13*, 175-182.

20. Kohn, S. C.; Michael, C.; Henderson, B.; Dupree, R. Si-Al Ordering in Leucite Group Minerals and Ion-Exchanged Analogues: An MAS NMR Study. *Am. Mineral.* **1997**, *82*, 1133-1140.

21. Engelhardt, G. in *Solid-State NMR Spectroscopy of Inorganic Materials,* Ed. J. J. Fitzgerald, **1999**, *ACS Symposium Series 717*, American Chemical Society, Washington, 266-282.

22. Müller, D.; Jahn, E.; Ladwig, G.; Haubenreisser, U. High-Resolution Solid-State ^{27}Al and ^{31}P NMR: Correlation between Chemical Shift and Mean Al-O-P Angle in $AlPO_4$ Polymorphs. *Chem. Phys. Lett.* **1984**, *109*, 332-336.

23. Gibbs, G. V. Molecules as Models for Bonding in Silicates. *Am. Mineral.* **1982**, *67*, 421-450.

24. Janes, N.; Oldfield, E. Prediction of Silicon-29 Nuclear Magnetic Resonance Chemical Shifts Using a Group Electronegativity Approach: Applications to Silicate and

Aluminosilicate Structures. *J. Am. Chem. Soc.* **1985**, *107*, 6769-6775.

25. Sherriff, B. L.; Grundy, H. D.; Hartman, J. S. Occupancy of T Sites in the Scapolite Series; a Multinuclear NMR Study Using Magic-Angle Spinning. *Can. Mineral.* **1987**, *25*, 717-730.

26. Sherriff, B. L.; Grundy, H. D.; Hartman, J. S. The Relationship between ^{29}Si MAS NMR Chemical Shift and Silicate Mineral Structure. *Eur. J. Mineral.* **1991**, *3*, 751-768.

27. Brown, I. D.; Altermatt, D. Bond-Valence Parameters Obtained from a Systematic Analysis of the Inorganic Crystal Structure Database. *Acta Cryst.* **1985**, *B41*, 244-247.

28. Bonhomme, C.; Gervais, C.; Laurencin, D. Recent NMR Developments Applied to Organic–Inorganic Materials. *Prog. Nucl. Magn. Reson. Spectrosc.* **2014**, *77*, 1-48.

29. Ashbrook, S. E.; McKay, D. Combining Solid-State NMR Spectroscopy with First-Principles Calculations – a Guide to NMR Crystallography. *Chem. Comm.* **2016**, *52*, 7186-7204.

30. Charpentier, T. The PAW/GIPAW Approach for Computing NMR Parameters: a new Dimension Added to NMR Study of Solids. *Solid State Nucl. Magn. Reson.* **2011**, *40*, 1-20.

31. Bonhomme, C.; Gervais, C.; Babonneau, F.; Coelho, C.; Pourpoint, F.; Azaïs, T.; Ashbrook, S. E.; Griffin, J. M.; Yates, J. R.; Mauri, F.; Pickard, C. J. First-Principles Calculation of NMR Parameters Using the Gauge Including Projector Augmented Wave Method: a Chemist's Point of View. *Chem. Rev.* **2012**, *112*, 5733-5779.

32. Ashbrook, S. E.; Dawson, D. M. Exploiting Periodic First-Principles Calculations in NMR Spectroscopy of Disordered Solids. *Acc. Chem. Res.* **2013**, *46*, 1964-1974.

33. Moran, R. F.; Dawson, D. M.; Ashbrook, S. E. Exploiting NMR Spectroscopy for the Study of Disorder in Solids. *Int. Rev. Phys. Chem.* **2017**, *36*, 39-115.

34. Ashbrook, S. E.; Dawson, D. M.; Griffin, J. M. in *Local Structure Characterisation*, **2014**, John Wiley & Sons, Ltd.

35. Dawson, D. M.; Ashbrook, S. E. Investigating Relationships between the Crystal Structure and [31]P Isotropic Chemical Shifts in Calcined Aluminophosphates. *J. Phys. Chem. C* **2014**, *118*, 23285-23296.

36. Frisch, M. J. *et al.* Gaussian 03, revision D.01; Gaussian, Inc.: Wallingford, CT, **2004**.

37. Jensen, F. Basis Set Convergence of Nuclear Magnetic Shielding Constants Calculated by Density Functional Methods. *J. Chem. Theory Comput.* **2008**, *4*, 719−727.

38. Clark, S. J.; Segall, M. D.; Pickard, C. J.; Hasnip, P. J.; Probert, M. J.; Refson, K.; Payne,

M. First Principles Methods Using CASTEP. *Z. Kristallogr.* **2005**, *220*, 567−570.

39. Pickard, C. J.; Mauri, F. All-Electron Magnetic Response with Pseudopotentials: NMR Chemical Shifts. *Phys. Rev. B* **2001**, *63*, 245101.

40. Perdew, J. P.; Burke, K.; Ernzerhof, M. Generalized Gradient Approximation Made Simple. *Phys. Rev. Lett.* **1996**, *77*, 3865−3868.

41. Yates, J. R.; Pickard, C. J.; Mauri, F. Calculation of NMR Chemical Shifts for Extended Systems Using Ultrasoft Pseudopotentials. *Phys. Rev. B* **2007**, *76*, 024401.

42. Fyfe, C. A.; Grodney, H.; Feng, Y.; Kokotailo, G. T. Natural-Abundance Two-Dimensional ^{29}Si MAS NMR Investigation of the Three-Dimensional Bonding Connectivities in the Zeolite Catalyst ZSM-5. *J. Am. Chem. Soc.*, **1990**, *112*, 8812-8820.

43. Morris, R. E.; Weigel, S. J.; Henson, N. J.; Bull, L. M.; Janicke, M. T.; Chmelka, B. F.; Cheetham, A. K. A Synchrotron X-ray Diffraction, Neutron Diffraction, ^{29}Si MAS-NMR, and Computational Study of the Siliceous Form of Zeolite Ferrierite. *J. Am. Chem. Soc.*, **1994**, *116*, 11849-11855.

44. MATLAB and Statistics Toolbox Release 2011b, The MathWorks, Inc., Natick, MA.

45. Baerlocher, C.; McCusker, L. B. *Database of Zeolite Structures*: http://www.iza-structure.org/databases/

46. Wragg, D. S.; Morris, R. E.; Burton, A. W. Pure Silica Zeolite-type Frameworks: a Structural Analysis. *Chem. Mater.*, **2008**, *20*, 1561-1570.

47. Bull, I.; Lightfoot, P.; Villaescusa, L. A.; Bull, L. M.; Gover, R. K. B.; Evans, J. S. O.; Morris, R. E. An X-ray Diffraction and MAS NMR Study of the Thermal Expansion Properties of Calcined Siliceous Ferrierite. *J. Am. Chem. Soc.*, **2003**, *125*, 4342-4349.

48. van Konningsveld, H.; Jansen, J. C.; van Bekkum, H. The Monoclinic Framework Structure of Zeolite H-ZSM-5. Comparison with the Orthorhombic Framework of As-Synthesized ZSM-5. *Zeolites*, **1990**, *10*, 235-242.

49. Brescani-Pahor, N.; Calligaris, M.; Nardin, G; Randaccio, L. Structure of a Basic Cancrinite. *Acta Cryst.* **1982**, *B38*, 893-895.

50. Le Page, Y.; Donnay, G. Refinement and Crystal Structure of Low-Quartz. *Acta Cryst.* **1976**, *B32*, 2456-2459.

51. Baur, W. H. Silicon-Oxygen Bond Lengths, Bridging Angles Si-O-Si and Synthetic Low Tridymite. *Acta Cryst.* **1977**, *B33*, 2615-2619.

52. Gard, J. A.; Tait, J. M. The Crystal Structure of the Zeolite Offretite,

$K_{1.1}Ca_{1.1}Mg_{0.7}[Si_{12.8}Al_{5.2}O_{36}].15.2H_2O$. *Acta. Cryst.* **1972**, *B28*, 825-834.

53. Kerr, I. S. Crystal Structure of a Synthetic Lithium Zeolite. *Z. Kristallogr.* **1974**, *139*, 186-195.

54. Olson, D. H. Reinvestigation of the Crystal Structure of the Zeolite Hydrated NaX. *J. Phys. Chem.* **1970**, *74*, 2758-2764.

55. Dollase, W. A. Reinvestigation of the Structure of Low Cristobalite. *Z. Kristallogr.* **1965**, *121*, 369-377.

56. Brown, B. E.; Bailey S. W. The Structure of Maximum Microcline. *Acta. Cryst.* **1964**, *17*, 1391-1400.

57. Peacor, D. R. High-Temperature, Single-Crystal X-Ray Study of Natrolite. *Am. Mineral.* **1973**, *58*, 676-680.

58. Gramlich, V.; Meier, W. M. The Crystal Structure of Hydrated NaA : a Detailed Refinement of a Pseudosymmetric Zeolite Structure. *Z. Kristallogr.* **1971**, *133*, 134-149.

59. Baerlocher, C.; Meier, W. M. Synthese und Kristallstruktur von Tetramethylammonium-Gismondin. *Helv. Chim. Acta* **1969**, *52*, 1853-1860.

60. Hassan, I.; Grundy, H. D. The Crystal Structures of Sodalite-Group Minerals. *Acta Cryst.* **1984**, *B40*, 6-13.

61. Gallezot, P.; Beaumont, R.; Barthomeuf, D. Crystal Structure of a Dealuminated Y-Type Zeolite. *J. Phys. Chem.* **1974**, *78*, 1550-1553.

62. Pant, A. K.; Cruikshank, D. W. J. The Crystal Structure of α-$Na_2Si_2O_5$. *Acta Cryst.* **1968**, *B24*, 13-19.

63. Pant, A. K. A Reconsideration of the Crystal Structure of β-$Na_2Si_2O_5$. *Acta Cryst.* **1968**, *B24*, 1077-1083.

64. Hassan, I.; Grundy, H. D. Structure of Basic Sodalite, $Na_8Al_6Si_6O_{24}(OH)_2.2H_2O$. *Acta Cryst.* **1983**, *C39*, 3-5.

65. Beagley, B.; Henderson, C. M. B.; Taylor, D. The Crystal Structures of Aluminosilicate-Sodalites: X-Ray Diffraction Studies and Computer Modelling. *Mineral. Mag.* **1982**, *46*, 459-464.

66. Pluth, J. J.; Smith, J. V. Neutron Diffraction Study of the Zeolite Thomsonite. *Zeolites* **1985**, *5*, 74-80.

67. Martucci, A.; Alberti, A.; Guzman-Castillo, M. L.; di Renzo, F.; Fajula, F. Crystal Structure of Zeolite Omega, the Synthetic Counterpart of the Natural Zeolite Mazzite.

Micropor. Mesopor. Mater. **2003**, *63*, 33-42.

68. Gibbs, G. V.; Prewitt, C. T.; Baldwin, K. J. A Study of the Structural Chemistry of Coesite. *Z. Kirstallogr.* **1977**, *145*, 108-123.

69. Harlow, G. E.; Brown, G. E. Low Albite - an X-Ray and Neutron-Diffraction Study. *Am. Mineral.* **1980**, *65*, 986-995.

70. Mortier, W. J.; Pluth, J. J.; Smith, J. V. Positions of Cations and Molecules in Zeolites with Chabazite Framework .1. Dehydrated Ca-Exchanged Chabazite. *Mater. Res. Bull.* **1977**, *12*, 97-102.

71. Schlenker, J. L.; Pluth, J. J.; Smith, J. V. Positions of Cations and Molecules in Zeolites with the Mordenite Framework .9. Dehydrated H-Mordenite via Acid Exchange. *Mater. Res. Bull.* **1979**, *14*, 849-856.

72. Mortier, W. J.; van den Bossche, E.; Uytterhoeven, J. B. Influence of the Temperature and Water-Adsorption on the Cation Location in Na-Y Zeolites. *Zeolites* **1984**, *4*, 41-44.

73. Sneddon, S.; Dawson, D. M.; Pickard, C. J.; Ashbrook, S. E. Calculating NMR Parameters in Aluminophosphates: Evaluation of Dispersion Correction Schemes. *Phys. Chem. Chem. Phys.* **2014**, *16*, 2660-2673.

Tables

Table 1. Relationships describing the systematic variation of Si–O–Si bond angles ($\theta_{SiOSi(i)}$), in the series of model Si(OSi(OH)$_3$)$_4$ clusters studied here (see Figure 2(a) for an example). The angles are expressed for the nth member of the series, and the number of clusters in the series, N, is given. For the central SiO$_4$ tetrahedron, the Si-O bonds were fixed at 1.62 Å and the O–Si–O angles at 109.47°.

Series	$\theta_{SiOSi(i)}$ (°)	N
1	$\theta_{SiOSi(1)} = \theta_{SiOSi(2)} = \theta_{SiOSi(3)} = \theta_{SiOSi(4)} = \langle\theta_{SiOSi}\rangle = 115 + 5n$	12
2	$\theta_{SiOSi(1)} = \theta_{SiOSi(2)} = 140$ $\theta_{SiOSi(3)} = 140 + 5n$ $\theta_{SiOSi(4)} = 140 - 5n$	7
3	$\theta_{SiOSi(1)} = \theta_{SiOSi(2)} = 140 + 5n$ $\theta_{SiOSi(3)} = \theta_{SiOSi(4)} = 140 - 5n$	6
4	$\theta_{SiOSi(1)} = 105 + 5n$ $\theta_{SiOSi(2)} = \theta_{SiOSi(3)} = \theta_{SiOSi(4)} = 140 + (140 - \theta_{SiOSi(1)})/3$	15
5	$\theta_{SiOSi(1)} = 150$ $\theta_{SiOSi(2)} = 105 + 5n$ $\theta_{SiOSi(3)} = \theta_{SiOSi(4)} = (410 - \theta_{SiOSi(2)})/2$	9
6	$\theta_{SiOSi(1)} = 120$ $\theta_{SiOSi(2)} = 175 - 5n$ $\theta_{SiOSi(3)} = \theta_{SiOSi(4)} = (440 - \theta_{SiOSi(2)})/2$	13
7	$\theta_{SiOSi(1)} = 105 + 5n$ $\theta_{SiOSi(2)} = \theta_{SiOSi(3)} = \theta_{SiOSi(4)} = 140$	15
8	all angles randomly generated,[a] $107.06 \leq \theta_{SiOSi(i)} \leq 174.96$	20

[a] For a full list of the randomly-generated angles, see the Supporting Information (S2).

Table 2. Relationships describing the systematic variation of Si–O bond lengths ($r_{SiO(i)}$), in the series of model $Si(OSi(OH)_3)_4$ clusters studied here (see Figure 2a for an example). The lengths are expressed for the nth member of the series, and the number of clusters in the series, N, is given. For the central SiO_4 tetrahedron, the O–Si–O angles were fixed at 109.47° and all Si–O–Si bond angles were fixed at 140°.

Series	$r_{SiO(i)}$ / Å	N
9	$r_{SiO(1)} = r_{SiO(2)} = r_{SiO(3)} = r_{SiO(4)} = \langle r_{SiO} \rangle = 1.61 + 0.01n$	15
10	$r_{SiO(1)} = r_{SiO(2)} = 1.62$ $r_{SiO(3)} = 1.61 + 0.01n$ $r_{SiO(4)} = 1.63 – 0.01n$	7
11	$r_{SiO(1)} = r_{SiO(2)} = 1.61 + 0.01n$ $r_{SiO(3)} = r_{SiO(4)} = 1.63 – 0.01n$	7
12	$r_{SiO(i)} = 1.56 + 0.01n$ $r_{SiO(2)} = r_{SiO(3)} = r_{SiO(4)} = 1.62$	10
13	all lengths randomly generated,[a] $1.45 \leq r_{SiO(i)} \leq 1.85$	40

[a] For a full list of the randomly-generated lengths, see the Supporting Information (S2).

Figures and Captions
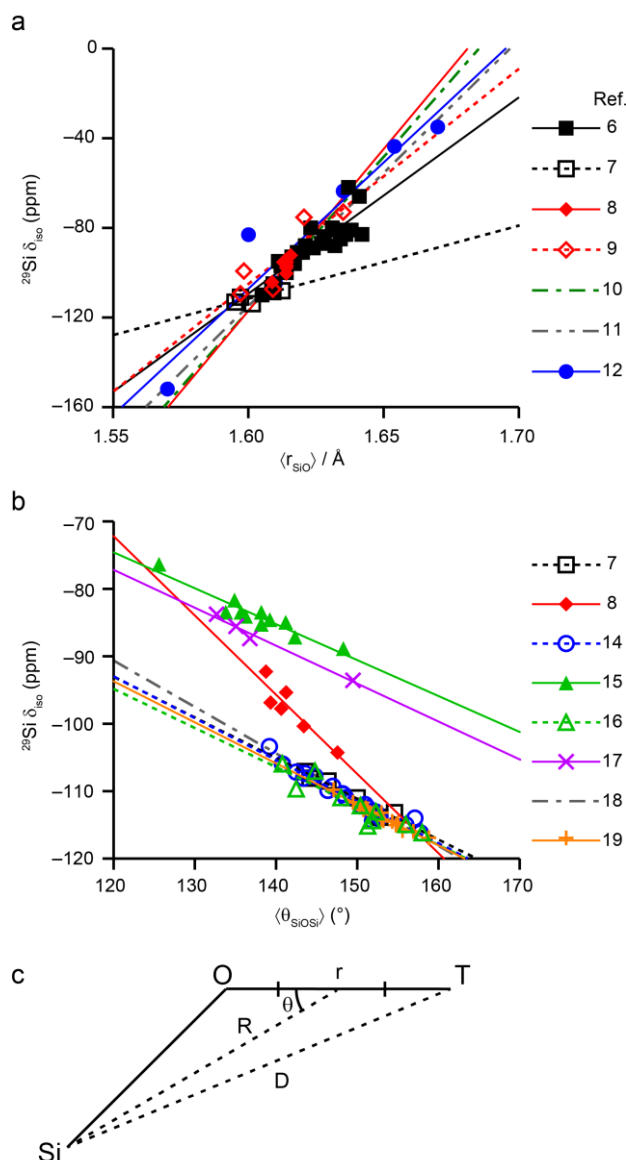
Figure 1. Plots of published relationships between [29]Si chemical shift and (a) mean Si–O bond length[6-12] and (b) mean Si–O–Si bond angles.[7,8 14-19] The lines represent lines of best fit to the experimental data (where data are available). Experimental data are not shown for Ref. 11, which is a re-analysis of existing literature data and determined the relationship indicated by the broken grey line in (a), and Ref. 18, where the data points are all included in the analysis of Ref. 16, but the relationship discussed in the main text is shown as the broken grey line in (b). Experimental data are not available for Ref. 10 (green line in (a)), which is a conference abstract and the numerical values do not appear to have been published elsewhere since. (c) Schematic representation of a general Si–O–T motif, showing the distances and angles used by Sherriff *et al.* to calculate the contribution to δ_{iso} from the dipole moment of the O–T bond.[26]
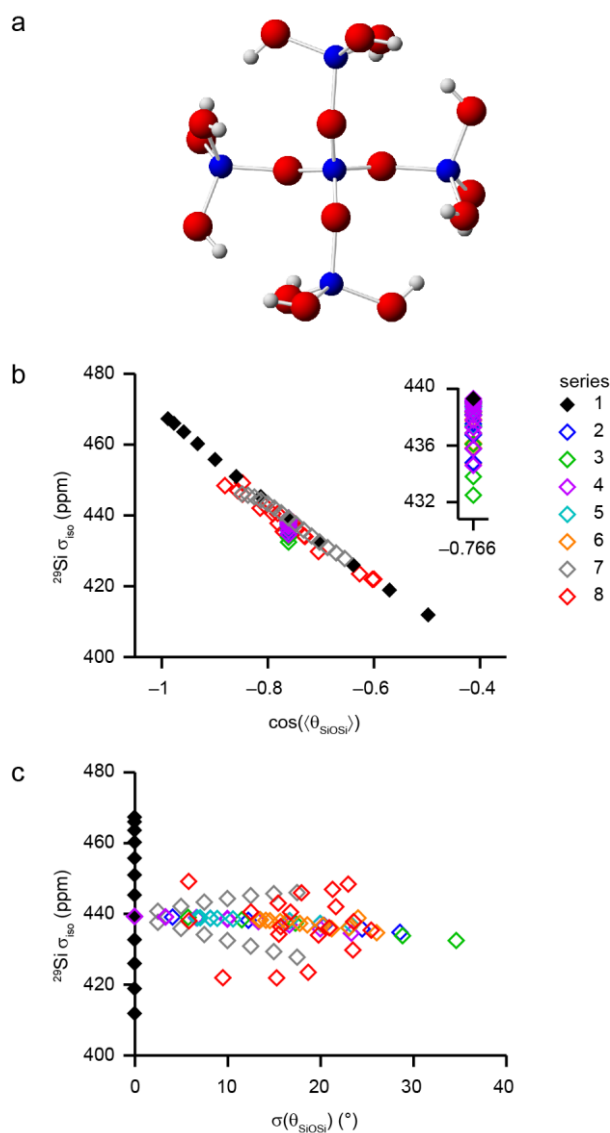
Figure 2. (a) Example of a $Si(OSi(OH)_3)_4$ cluster used to investigate the dependence of ^{29}Si σ_{iso} on the systematic variation of the structural parameters, $\langle\theta_{SiOSi}\rangle$ and $\langle r_{SiO}\rangle$. Atoms are coloured blue (Si), red (O) and grey (H). Plots of ^{29}Si σ_{iso} calculated for $Si(OSi(OH)_3)_4$ clusters against (b) $\cos(\langle\theta_{SiOSi}\rangle)$ and (c) $\sigma(\theta_{SiOSi})$. For details of the bond angles used in the model clusters, see Table 1. The inset in (b) shows only values for series 2-6, and series 1 (n = 5), with $\langle\theta_{SiOSi}\rangle = 140°$.
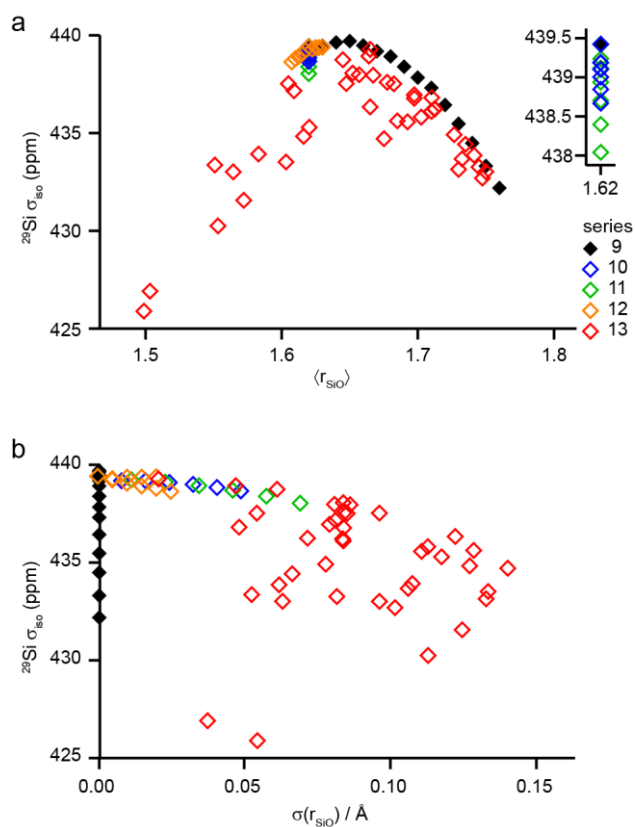
Figure 3. Plots of ^{29}Si σ_{iso} calculated for $Si(OSi(OH)_3)_4$ clusters against (a) $\langle r_{SiO} \rangle$ and (c) $\sigma(r_{SiO})$. For details of the bond lengths used in the model clusters, see Table 2. The inset in (a) shows only values for series 10 and 11, and series 9 (n = 1), with $\langle r_{SiO} \rangle$ = 1.62 Å.
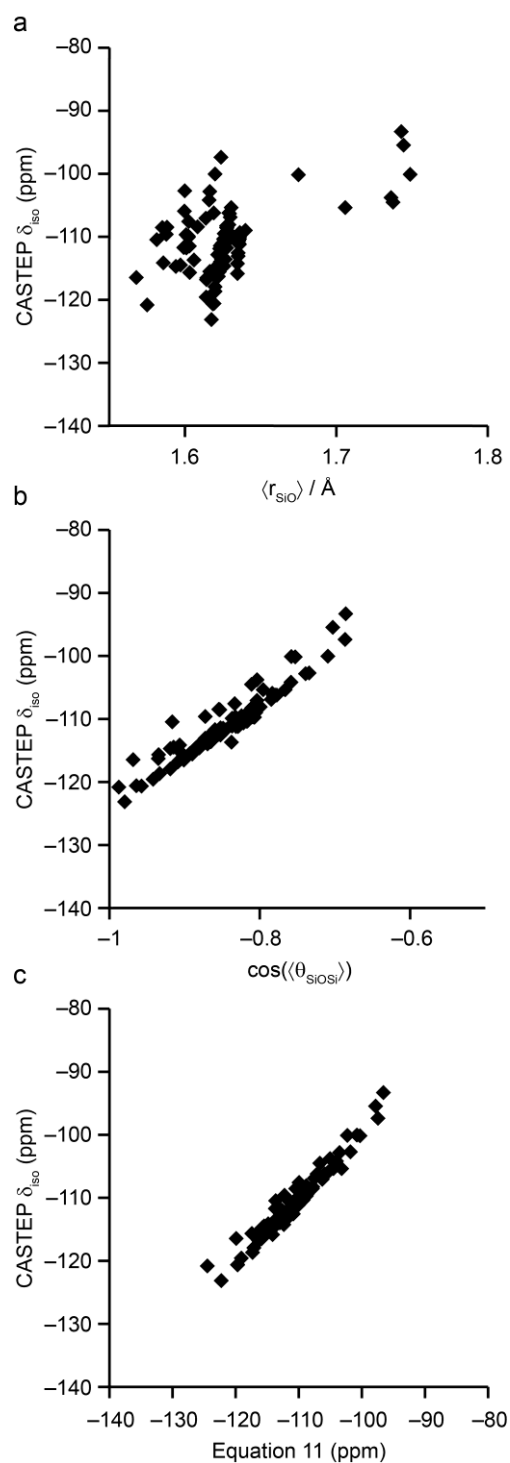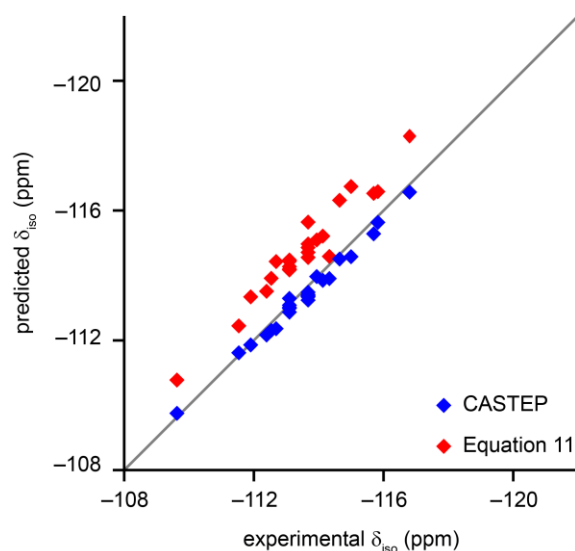
Figure 4. Plots of δ_{iso} calculated by CASTEP against (a) $\langle r_{SiO} \rangle$, (b) $\cos(\langle \theta_{SiOSi} \rangle)$ and (c) δ_{iso} predicted from the structure by Equation 11 for the series of 16 model zeolitic SiO_2 frameworks discussed in the text.
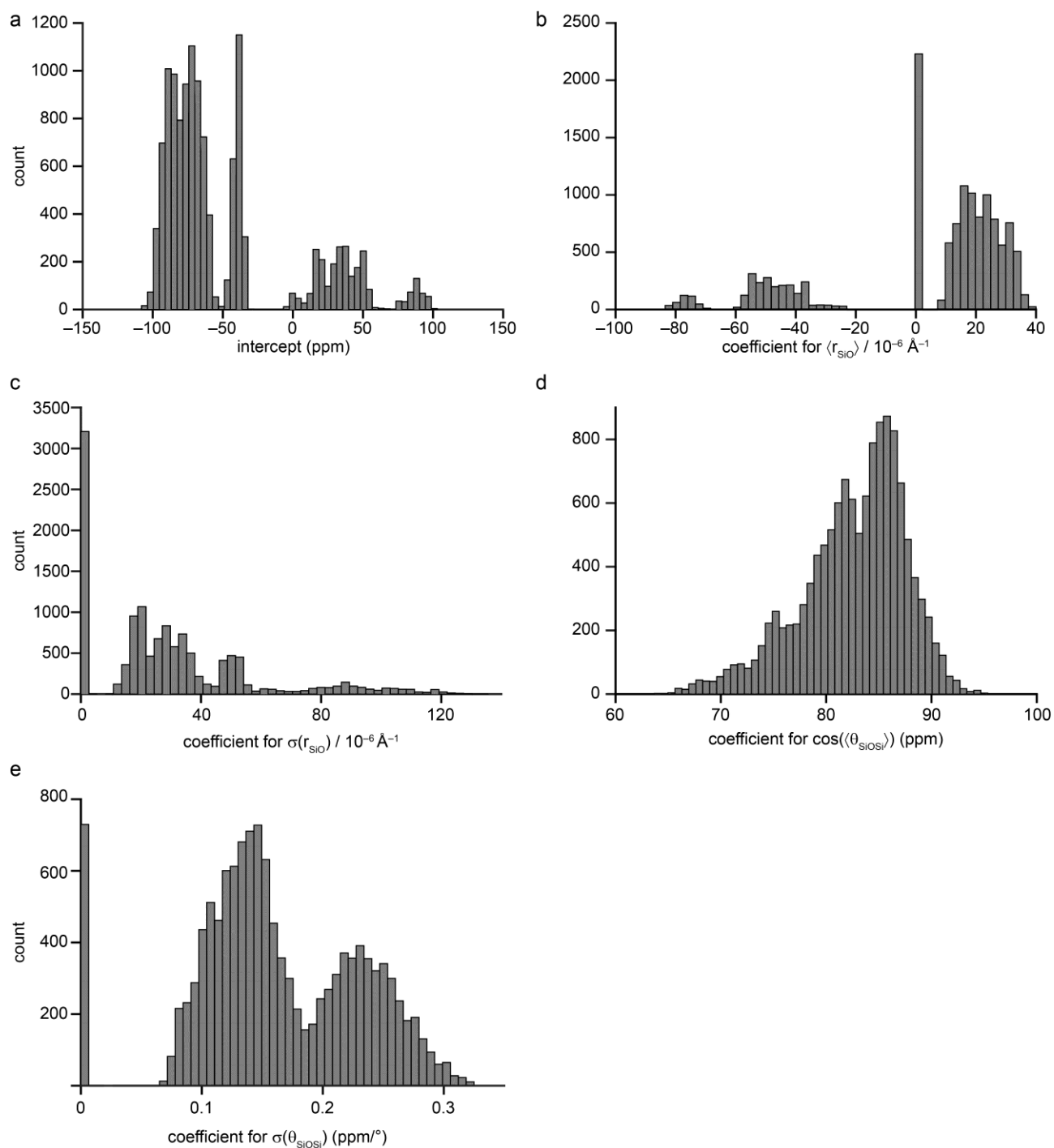
Figure 5. Histograms showing the distribution of values for the coefficients in Equation 11. The values were determined by repeating the parameterisation of Equation 11 for each of the 12870 possible combinations of 8 of the 16 model SiO_2 frameworks as described in the Supporting Information (S1).
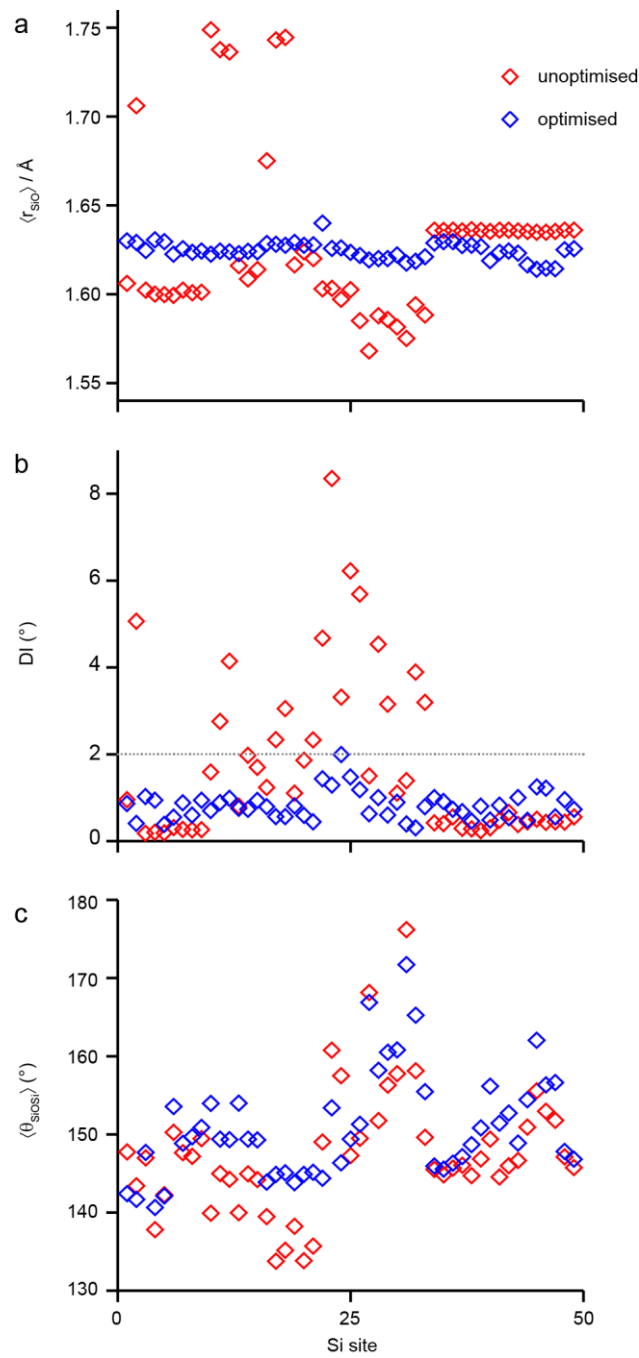
Figure 6. Plots of (a) $\langle r_{SiO} \rangle$, (b), distortion index, DI, and (c) $\langle \theta_{SiOSi} \rangle$ for the set of model silicate framework structures discussed in the main text before (red) and after (blue) optimisation using CASTEP. In (b), the dotted grey line indicates the threshold of DI = 2.0°. In all parts, the x axis serves only to separate the distinct Si species.

Figure 7. Plots of ^{29}Si δ_{iso} predicted by Equation 11 (red points) and calculated by CASTEP (blue points), against the experimental values[42] for SiO$_2$-MFI. The grey line indicates the ideal 1 : 1 correspondence.
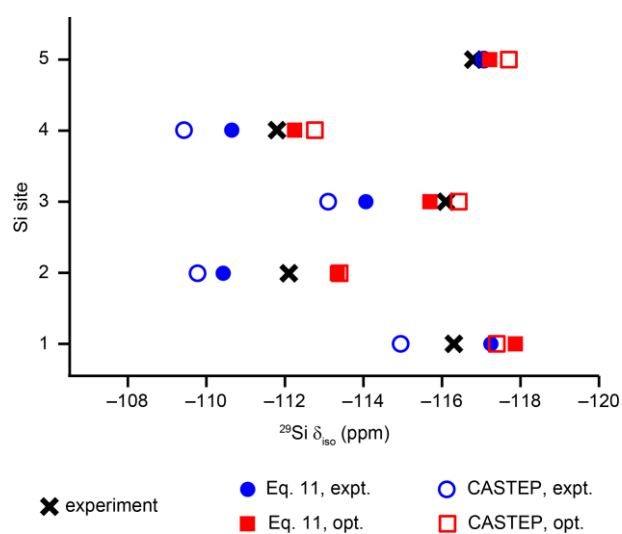
Figure 8. Plots of ^{29}Si δ_{iso} for the five Si sites in SiO$_2$-FER. Experimental values (from Morris *et al.*[43]) are shown by crosses, values calculated by Equation 11 are shown by filled shapes and empty shapes show values calculated by CASTEP. The values are calculated from the experimental structure (expt., circles), and the DFT-optimised structure (opt., squares).
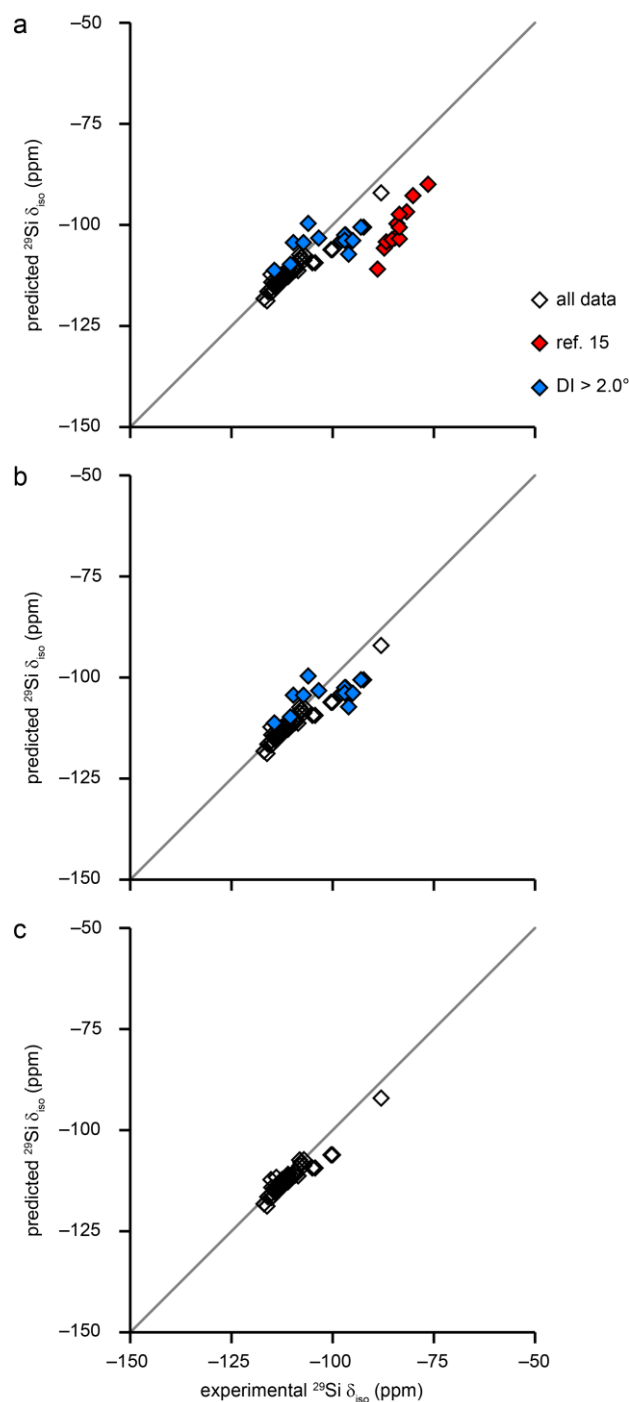
Figure 9. Plots of ^{29}Si δ_{iso} predicted by Equation 11 against the experimental values for the tectosilicates shown in Figure 1. [7,8,14-16] (a) Plot including all reported data points, with the red points corresponding to $Si(OAl)_4$ sites reported by Newsam.[15] (b) The same plot as part (a), but with the red points omitted. The blue points correspond to structures with a distortion index greater than 2.0°. (c) The same plot as part (b), but with the blue points omitted. For all parts, structural parameters were taken from the literature references cited in the original spectroscopic works, where possible.[48-72] Further details are given in the Supporting Information (S6). The grey lines indicate the ideal 1 : 1 correspondence.

TOC Graphic